ARTICLE NO. 78-1337

Prediction of Roll Controllability of Slender Cruciform Canard Configurations

I. Gur,* J. Shinar,† and J. Rom‡
Technion – Israel Institute of Technology, Haifa, Israel

Canard configurations having modular flexibility are attractive candidates for modern guided weaponry. Roll control of such configurations requires careful aerodynamic design. Elaborate computations are, however, prohibitive. The paper presents a simplified mathematical model predicting induced rolling moments of slender cruciform canard configurations with reasonable engineering accuracy. It is based on a classical vortex model improved by considering tail-body interference both on vortex trajectories and the roll influence function. Comparison to wind-tunnel data at $M=2.25$ for small angles of attack was satisfactory. The method can be extended for higher angles of attack and to include computation of induced forces and lateral moments.

Nomenclature

a = body radius
b = full span of lifting surface
c = lifting surface root chord
C_F = force coefficient $= F/QS$
C_L = rolling moment coefficient $= L/QSd$
d = body diameter
F = aerodynamic force
F_c = induced roll influence coefficient, Eqs. (33) and (34)
$K_{B(w)}, K_{w(B)}$ = interference coefficients
l_N = nose length
l_t = the distance between the trailing edge of the canard and the trailing edge of the tail
L = rolling moment
M = Mach number
n = number of successive cross-flow planes for trajectory calculation
p = polar coordinate in the physical plane
Q = dynamic pressure
q = dimensionless coordinate in the transformed plane
r = distance between two vortices
R = radius of the circle in transformed plane
s = semispan (including body radius)
S = reference area
t = time
$v-iw$ = velocity in the transformed cross-flow plane
$\hat{v}-i\hat{w}$ = velocity in the physical cross-flow plane
V_o = freestream velocity
W = complex potential
x = coordinate along body axis
X = complex coordinate $= y+iz$
y,z = spanwise coordinates
α = angle of attack
Γ = vorticity strength
δ = control surface deflection
η,ζ = Cartesian coordinates in the transformed plane
θ = angular coordinate in the physical plane
ρ = freestream air density
σ = nondimensional coordinate $= \Sigma/R$
Σ = complex coordinate $= \eta+i\zeta$
ϕ = polar coordinate in the transformed plane
Φ = velocity potential
Φ' = normalized potential, Eq. (A12)
ψ = stream function

Subscripts

c = canard
c.f = cross-flow
i = induced
p = pitch
R = roll
t = tail
y = yaw
v = vortex
0 = initial

Submitted June 29, 1978; presented as Paper 78-1337 at the AIAA Atmospheric Flight Mechanics Conference, Palo Alto, Calif., Aug. 7-9, 1978; revision received Dec. 7, 1978.

Index categories: LV/M Configurational Design; LV/M Dynamics and Control.

*Graduate Student, Dept. of Aeronautical Engineering.
†Associate Professor, Dept. of Aeronautical Engineering. Member AIAA.
‡Professor, Lady Davis Chair of Experimental Aerodynamics. Associate Fellow AIAA.

Introduction

SIGNIFICANT renewed interest has been given to canard-controlled configurations, due to the modular flexibility provided by such design. Some of the missions for which the modular design is attractive require roll stabilization. In the past canard surfaces were rarely used for roll control. The asymmetric flowfield created by differential deflections of the canard fins induces an adverse rolling moment on the tail surfaces. This induced rolling moment is very often larger in magnitude than the original one. It has been demonstrated, however, that by careful aerodynamic considerations roll-controllable cruciform canard configurations can be designed.[1]

There exist today some elaborate methods to compute the exact flowfield behind the canard surfaces. These numerical methods require an excessive amount of computation, which is prohibitive in the preliminary design process.

In this paper a simple mathematical model is presented, which enables prediction of induced rolling moments of slender canard configurations with reasonable engineering accuracy. The simplicity of the model is a consequence of the following set of assumptions:

1) Control deflections and angles of incidence are small. Thus, force and moment coefficients can be considered linear. Moreover, body and leading-edge vortices can be neglected.

2) The aerodynamic load of each control surface can be represented by a single fully rolled up infinite vortex and its image. This assumption requires that the distance between the canard trailing edge and the leading edge of the rear lifting surface be greater than the canard's root cord.[2]

3) The velocity along the x axis of the body is constant and equal to the freestream velocity.

4) The tail lifting surface is of very low aspect ratio; thus the roll influence function can be calculated at the trailing-edge section.

These assumptions are by no means new. They were used in the past in several studies. The first relevant work of this nature was that of Edwards and Hikido.[3] It was based on a semigraphical approach which required extreme simplifications: the influence of the rear lifting surfaces on vortex trajectories was neglected, and roll influence functions were calculated only for cruciform (bodyless) wings. Both assumptions may yield, as has been demonstrated recently,[4] seriously misleading predictions.

In the 1950's, several reports were written dealing with the canard-induced flowfield in cruciform configurations.[5-7] Their results were synthesized to an applicable methodology in the excellent textbook of Nielsen.[8] Since then, only a few known works have addressed the problem of induced rolling moment predictions. Some authors proposed to improve the mathematical model by representing the canard surfaces by several discrete vortices. Udelson[9] presented a closed-form solution applicable to planar tail-body combinations.

A new methodology was recently introduced by Mendenhall and Nielsen[10] to compute the induced flowfield in wing-body-tail combinations. Their work is oriented toward predicting longitudinal aerodynamic characteristics of aircraft configurations. This rather elaborate method of computation, based on lifting surface theory, is unfortunately not directly applicable to cruciform designs. Neither can it be used to predict induced lateral forces and moments.

In this paper a more simple mathematical model is used, taking into account, however, the tail-body interference, neglected in past studies,[3] both on the vortex trajectories and induced roll moment influence functions. Predicted results are compared to wind-tunnel measurements on a slender interdigitated cruiciform configuration (see Fig. 1).

Mathematical Model

The prediction of the induced rolling moment is carried out by the following steps:

1) Calculation of the aerodynamic load due to angles of incidence and control deflection on each of the canard surfaces.

2) Computation of the strength and position of the single vortex representing the load (see assumption 2) and the definition of the image vortex to satisfy the boundary conditions of "no flow through the body."

3) Calculation of the downstream trajectory of all vortices in the presence of the body and the tail.

4) Estimation of the rolling moment induced by each of the vortices on the tail-body combination.

The first two steps are carried out by well-known classical methods. The last phases are those in which an innovative approach is introduced, leading to major improvement.

Load on the Canard Surfaces

The aerodynamic load of the canard surfaces is due to three separate sources:

1) Angle of attack (or sideslip) generating symmetrical loading on the opposite surfaces (i.e., zero rolling moment).

2) Symmetrical control deflection of a pair of surfaces creating equal forces and, as a consequence, zero rolling moment.

3) Differential deflection of the control surfaces resulting in a net rolling moment but zero total force.

On the basis of the assumption of small angles (assumption 1), we can assume linearity and superposition:

$$F(\alpha,\delta) = F(\alpha) + F(\delta) \tag{1}$$

$$L(\alpha,\delta) = L(\alpha) + L(\delta) \tag{2}$$

The control's deflections are defined as follows (Fig. 2).

Symmetrical deflections in the pitch plane:

$$\delta_p = (\delta_1 + \delta_3)/2 \tag{3}$$

Symmetrical deflections in the yaw plane:

$$\delta_y = (\delta_2 + \delta_4)/2 \tag{4}$$

Differential deflections creating a rolling moment:

$$\delta_R = (\delta_1 - \delta_2 - \delta_3 + \delta_4)/2 \tag{5}$$

The aerodynamic force due to angles of attack and symmetrical deflection in pitch or yaw can be calculated by any of the conventional methods, taking into account wing-body interference. The rolling moment was calculated by slender body theory[11] with appropriate corrections for non-slenderness, as suggested by Nielsen.[8]

Representation of the Aerodynamic Load by a Single Vortex and Its Image

The exact lift distribution of each canard fin is described rigorously by an infinite number of vortices, distributed along the span.

In our model the load of each lifting surface is represented by a single fully rolled-up vortex of strength Γ. This very important simplification is based on the result of Spreiter and Sacks,[5] who compared the wakes of 10 exterior vortices per fin to the wake of a single one and found a "remarkably good agreement at all distances behind the wing." The representative vortex is assumed to originate at the canard surface trailing edge.

In order to satisfy the boundary condition of "no flow through the body," each exterior vortex must have its "image" of the same strength but opposite direction. The position of the exterior vortex (y_v or z_v, respectively) and its image are related to each other by

$$y_{\text{im}} = a^2/y_v \qquad z_{\text{im}} = a^2/z_v \tag{6}$$

The relationship between the normal force and the strength of the fully rolled-up trailing vortex representing it can be written for each lifting surface (e.g., a horizontal one) as

$$F \triangleq \tfrac{1}{2}\rho V_0^2 S C_F = 2\rho V_0 \Gamma [y_v - (a^2/y_v)] \tag{7}$$

The rolling moment created by this normal force is therefore given by

$$L \triangleq \tfrac{1}{2}\rho V_0^2 S d C_L = \rho V_0 \Gamma [y_v^2 - (a^4/y_v^2)] \tag{8}$$

The lateral position of the vortex is so chosen that the load distribution due to angle of attack between the body and the lifting surface is truly represented, yielding

$$y_v = a[K_{w(B)}/K_{B(w)}] \tag{9}$$

Fig. 1 An interdigitated cruciform canard missile.

where $K_{w(B)}$ and $K_{B(w)}$ are the wing-body interference coefficients introduced by Nielsen.[8]

As a consequence of this choice the load distribution due to symmetrical control deflection is also represented with a good approximation.

It has to be noted, however, that Eqs. (7-9) do not represent correctly the aerodynamic load on the body due to differential control deflection. This error is of minor importance because this aerodynamic load on the body does not contribute either to the normal force or to the rolling moment.

The vortex strength is calculated by superposition (see the first assumption) of the symmetrical and antisymmetrical contributions:

$$\left(\frac{\Gamma}{V_0}\right)=\left(\frac{\Gamma}{V_0}\right)_{\text{sym}}+\left(\frac{\Gamma}{V_0}\right)_{\text{asym}} \tag{10}$$

The symmetrical contribution includes the effect of the normal force due to incidence and symmetrical control deflection:

$$\left(\frac{\Gamma}{V_0}\right)_{\text{sym}}=\frac{y_v S C_F}{4(y_v^2-a^2)} \tag{11}$$

with

$$C_F=C_{F_\alpha}\alpha+C_{F_\delta}\delta_{\text{sym}} \tag{12}$$

The antisymmetrical contribution is due to the rolling moment,

$$\left(\frac{\Gamma}{V_0}\right)_{\text{asym}}=\frac{y_v^2 S d C_L}{2(y_v^4-a^4)} \tag{13}$$

created by the differential control deflection;

$$C_L=C_{L_\delta}\delta_{\text{diff}} \tag{14}$$

It is important to note that in a cruciform configuration differential deflection of one pair of control surfaces has two effects: 1) creating a positive rolling moment due to the aerodynamic load distribution on the deflected surfaces, and 2) inducing an adverse rolling moment on the undeflected pair of surfaces.

Both rolling moment coefficients are given in Ref. 11 and are based on slender body theory as a function of the ratio (a/s).

Downstream Trajectory of the Vortices

Once the strength and position of all vortices are determined by Eqs. (6), (9), and (10)-(14), computation of the downstream trajectory can be initiated.

The three-dimensional motion of the vortices can be decomposed to 1) movement at a constant velocity V_0 in the direction of the freestream, and 2) movement in the cross-flow plane due to the up-wash created by the angle of attack and the mutual interference of the entire vortex system, both in the presence of the tail-body combination.

Neglecting the existence of the tail (which has been done previously[3,4]) may lead to the nonrealistic result that a vortex trajectory is intersected by one of the tail surfaces.

In this work the influence of the tail surfaces on vortex trajectories is taken into account by the following method. The double Joukowsky transformation,

$$X^2+a^4/X^2=\Sigma^2+R^4/\Sigma^2 \tag{15}$$

transforms a cruciform wing-body combination of radius a and half-span $s(x)$ into a circle of radius $R(x)$ (see Fig. 3):

$$R(x)=\frac{a}{\sqrt{2}}\left[\left(\frac{s(x)}{a}\right)^2+\left(\frac{a}{s(x)}\right)^2\right]^{1/2} \tag{16}$$

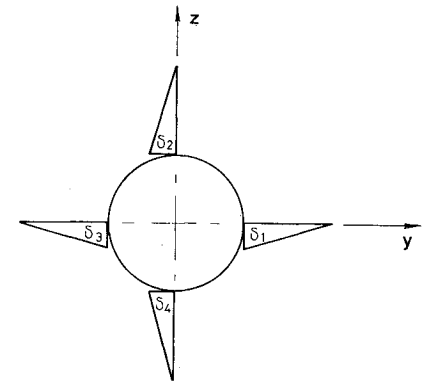

Fig. 2 Definition of control deflections.

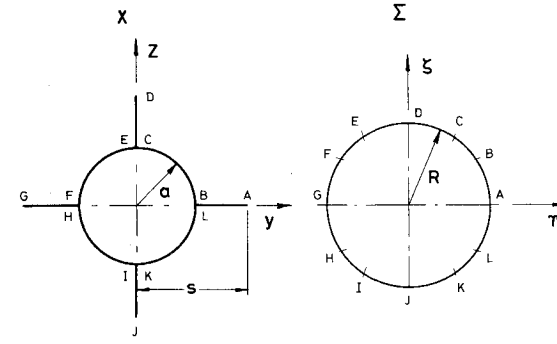

Fig. 3 Transformation of a cruciform wing-body section to a circle.

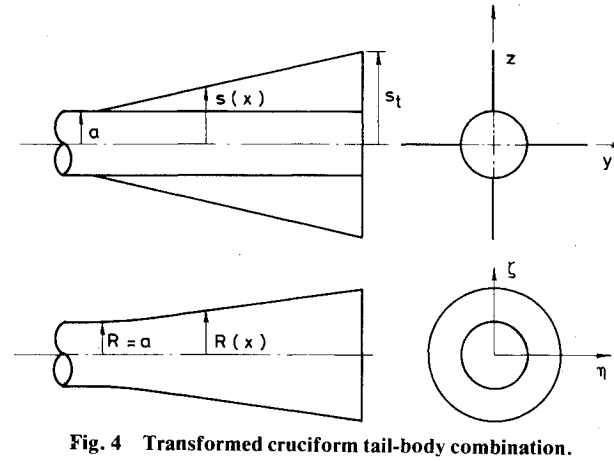

Fig. 4 Transformed cruciform tail-body combination.

For the cylindrical part of the configuration $[s(x)=a]$, we have also

$$R(x)\equiv a \tag{17}$$

Performing a successive transformation along the x axis of the configuration, a cylindrical body with a varying radius is obtained (see Fig. 4).

In the transformed domain the boundary conditions (no flow through the circle) are easily formulated. The image vortices inside the transformed body, which guarantee to satisfy the boundary conditions, also guarantee that no vortex trajectory will ever intersect any of the tail's surfaces. The transformation (15) is of course two-dimensional, and the transformed body is merely a collection of transformed cross-flow planes.

The velocity in the cross-flow plane is obtained from derivation of the complex potential:

$$v-iw=\mathrm{d}W/\mathrm{d}\Sigma \tag{18}$$

which is composed of

$$W = W_i + W_{c.f.} + W_a \tag{19}$$

where W_i is the potential induced by the vortices

$$W_i = \sum_{j=1}^{8} W_{i,j} = \sum_{j=1}^{8} \sum_{\substack{k=1 \\ k\neq j}}^{8} i\frac{\Gamma_k}{2\pi} \ln r_{jk} \tag{20}$$

with

$$r_{jk} = \Sigma_j - \Sigma_k \tag{21}$$

$W_{c.f.}$ is the cross-flow potential given by

$$W_{c.f.} = -V_0 \sin\alpha [\Sigma + (R^2/\Sigma)] \tag{22}$$

and W_a is the potential due to varying body radius. If, as in the present case, the configuration has a cylindrical body (see Fig. 4), W_a is equal to zero.

It is rather inconvenient to express the longitudinal component of the velocity in the transformed domain. It is simpler to transform the cross-flow component of the velocity back to the physical plane and to add it there to the longitudinal component. In this retransformation, the influence of each vortex on its own velocity must be taken into account, as was indicated by Nielsen,[8] using the first and second derivatives of the conformal transformation (15). The transversal velocity in the physical cross-flow plane is given by

$$\hat{v}_j - i\hat{w}_j = (v_j - w_j)\frac{d\Sigma}{dX}\bigg|_{x=x_j} - i\frac{\Gamma_j}{4\pi}\frac{d^2\Sigma/dX^2}{d\Sigma/dX}\bigg|_{x=x_j} \tag{23}$$

Vortex trajectory integration is carried out step by step, assuming that the transversal velocity remains constant for a short period of time, Δt:

$$\Delta t = l_t/nV_0 \tag{24}$$

n being the number of steps.

The trajectory components are

$$\Delta x_j = V_0(\Delta t) = (l_t/n) \tag{25}$$

$$\Delta y_j = \hat{v}_j(\Delta t) = (\hat{v}_j/V_0)\cdot(l_t/n) \tag{26}$$

$$\Delta z_j = \hat{w}_j(\Delta t) = (\hat{w}_j/V_0)\cdot(l_t/n) \tag{27}$$

Each step carries the vortices to the next tail-body section, which is again transformed to a circle. These steps are repeated in successive cross-flow sections along the tail-body combination until they reach the tail's trailing edge, where the roll influence function is computed. An example is shown in Fig. 5.

Induced Rolling Moment

The rolling moment of a slender configuration can be derived from the velocity potential of the flowfield Φ by the strip theory.[3,8,10] It gives for a single horizontal tail surface

$$L = -\rho V_0 \int_a^{s_t} (\Delta\Phi_{T.E.} - \Delta\Phi_{L.E.}) y\,dy \tag{28}$$

The expressions for the other tail surfaces are similar. For a triangular planform $(\Delta\Phi)_{L.E.} \equiv 0$ and therefore Eq. (28) is reduced to

$$L = -\rho V_0 \int_a^{s_t} (\Delta\Phi)_{T.E.} y\,dy \tag{29}$$

The velocity potential at the trailing-edge section of the tail is the sum of the potentials induced by the four pairs of conjugate vortices (four exterior trailing vortices and their images). If the cruciform tail-body section is transformed to a circle using Eq. (15), the nondimensional potential induced by a pair of conjugate vortices can be easily calculated (as shown in detail in the Appendix) as

$$\frac{\Phi}{\Gamma/2\pi} \triangleq \Phi' = \tan^{-1}\left\{\frac{[q_v - (1/q_v)]\sin(\phi-\phi_v)}{2 - [q_v + (1/q_v)]\cos(\phi-\phi_v)}\right\} \tag{30}$$

The potential is retransformed to the physical domain in nondimensional form

$$X' = y' + iz' = (y/s_t) + i(z/s_t) \tag{31}$$

which yields for the horizontal tail surfaces ($z=0$)

$$\phi(y') = \tfrac{1}{2}\cos^{-1}\left[\frac{y'^4 + (a/s_t)^4}{2y'^2(R/s_t)^2}\right] \tag{32}$$

and a similar expression for the vertical tail surface ($y=0$).

For each coordinate y' (or z'), two values of ϕ are obtained. The positive value corresponds to the upper surface of the tail and the negative one to the lower surface. The nondimensional potential difference at any point is given by

$$\Delta\Phi'(y') = \Phi'[\phi(y')] - \Phi'[-\phi(y')] \tag{33}$$

Integration is carried out mainly for numerical convenience in the physical plane. Substituting Eq. (32) and its equivalent into Eq. (30) leads to the following formula for the rolling moment induced on the cruciform tail-body combination by each pair of vortices:

$$L_j = \rho V_0 s_t^2 \frac{\Gamma_j}{2\pi}\left[\int_{a/s_t}^{1} \Delta\Phi'(y')y'\,dy' - \int_{a/s_t}^{1} \Delta\Phi'(z')z'\,dz' + \int_{-a/s_t}^{-1} \Delta\Phi'(y')y'\,dy' - \int_{-a/s_t}^{-1} \Delta\Phi'(z')z'\,dz'\right] \tag{34}$$

This induced rolling moment can be represented by a nondimensional roll influence function defined as

$$L_j \triangleq \rho V_0 s_t^2 (\Gamma_j/2\pi) F_c \tag{35}$$

with F_c being the sum of the four integrals in the brackets in Eq. (34). The value of F_c is determined by the position of the vortex (y_v', z_v') in the normalized coordinate system of the cruciform tail-body combination.

Once the induced rolling moment is calculated, the total rolling moment due to differential deflection of the canard control surfaces can be obtained by Eqs. (8) and (35):

$$L = L_0 + L_i = \tfrac{1}{2}\rho V_0^2 \sum_{j=1}^{4}\left(\frac{\Gamma_j}{V_0}\right)\left(\frac{y_{vj}^4 - a^4}{y_{vj}^2} + \frac{s_t^2}{\pi}F_{cj}\right) \tag{36}$$

The expression in the brackets indicates the roll controllability of the configuration. As it can be seen by inspection of Eq. (36), this controllability is strongly influenced by the value of the influence function. The characteristics of this function deserve detailed discussion in a separate section.

Influence Function Maps

As the value of the induced roll influence function F_c depends only on the nondimensional position of the vortex and on the lower limit of the integral in Eq. (34) a/s_t (the radius/semispan ratio at the tail trailing edge), maps exhibiting lines of "iso-F_c" can be constructed for each given value of this parameter. The construction is rather simple.

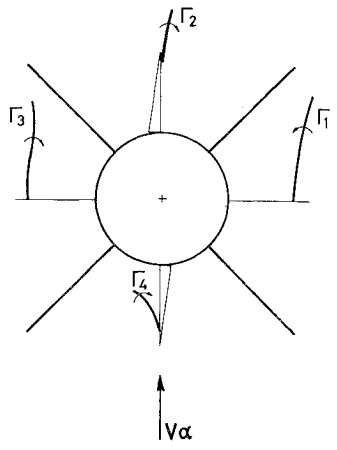

Fig. 5 Typical vortex trajectories.

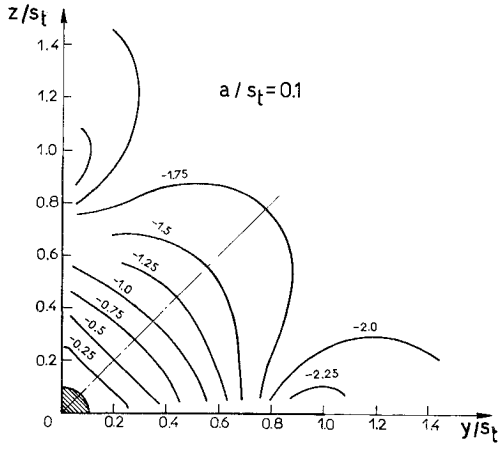

Fig. 6 Roll influence map, $a/s_t = 0.1$.

Due to considerations of symmetry in cruciform tail-body section, computation of F_c is carried out only for one octant. As indicative examples two such maps are shown in Figs. 6 and 7 for values of $a/s_t = 0.1$ and $a/s_t = 0.35$.

By inspecting these maps, some important conclusions can be obtained, providing insight into the complex phenomenon of the induced roll.

1) The roll influence function F_c due to a pair of conjugate vortices is always negative, i.e.; the induced rolling moment is adverse.

2) The value of F_c on the body is always zero because in this case the conjugate vortices cancel each other [see Eq. (6)].

3) Along the fins F_c has a strong gradient which is increasing toward the wing tip, where the value is theoretically infinite.

4) Along the line of symmetry between the fins, the absolute value of F_c is monotonically increasing, with the distance from the body reaching a limit.

5) The maximum of the absolute value of F_c (for vortex at infinity and its image at the center of the body) depends only on (a/s_t). This dependence is depicted in Fig. 8. For the ratio a/s_t approaching zero, the value obtained (-2.0) is equivalent to the result of Edwards and Hikido[3] obtained for cruciform wings.

6) Comparing Figs. 6 and 7 and inspecting Fig. 8 leads to the conclusion that the influence of the body on the roll influence function cannot be neglected. A larger body reduces significantly the induced rolling moment.

7) The value F_c for vortices near the tail surfaces is rather sensitive to the exact position, as can be seen in the cross plot presented in Fig. 9 for constant radials. It indicates that small

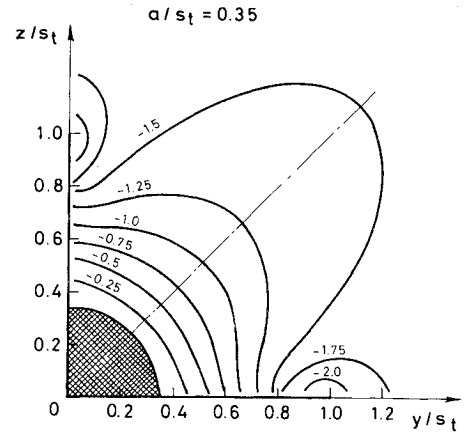

Fig. 7 Roll influence map, $a/s_t = 0.35$.

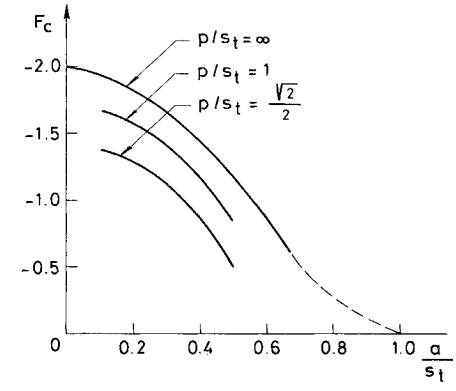

Fig. 8 Dependence of F_c on a/s_t at the line of symmetry.

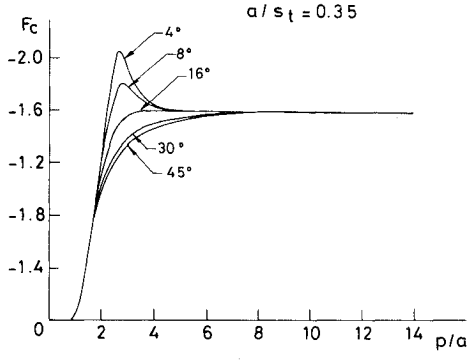

Fig. 9 Dependence of F_c on the vortex position for constant radials $(a/s_t = 0.35)$.

changes in angle of attack or sideslip can induce strong variations of the net rolling moment—situation that has to be avoided for efficient roll control.

These conclusions can be most useful in the aerodynamic design of a canard-controlled configuration. The influence maps themselves can serve as convenient tools in the preliminary phases of design.

Computation Example and Comparison to Wind-Tunnel Tests

To verify the accuracy of the mathematical model and computational procedure described in the previous section, an example for which relevant wind-tunnel test data exist was chosen. It happened to be an interdigitated cruciform canard missile with slender delta lifting surfaces. Wind-tunnel tests of such a configuration, very similar to the one shown in Fig. 1, were described in detail in a previous paper.[4]

The main characteristics of the configuration can be summarized as follows:

body slenderness ratio	$l/d=13.8$
canard aspect ratio	$\mathcal{R}_c=1.68$
canard semispan ratio	$a/s_c=0.44$
tail aspect ratio	$\mathcal{R}_t=0.91$
tail semispan ratio	$a/s_t=0.35$
relative trailing edge distance	$l_t/c_c=5.1$

This configuration was tested in the 40×50 cm supersonic wind tunnel of the Aeronautical Research Center at the Technion—Israel Institute of Technology. More than 40 test runs with different combinations of control deflections were carried out at Mach number 2.25 in the range of small angles of attack. The accuracy of the experimental data relating to rolling moment measurements has been estimated to be about 5-10%.

The computer program, which had been developed implementing all phases of induced rolling moment prediction described in this paper, was used for the existing data points. One computer run (for a given configuration at a fixed angle of attack) required less than 3 s c.p.u. on a CDC 6500. Comparison between experimental data, the predicted results obtained by both the present model, and the model of Ref. 3 is shown in Figs. 10 and 11 for vertical and horizontal canard control deflections, respectively.

Inspection of these figures indicates that the comparison can be considered more than satisfactory. Especially if one takes into account that Eq. (36) gives the resultant rolling moment as the difference between two larger quantities. The improvement achieved by the present method in comparison to that of Ref. 3 is obvious.

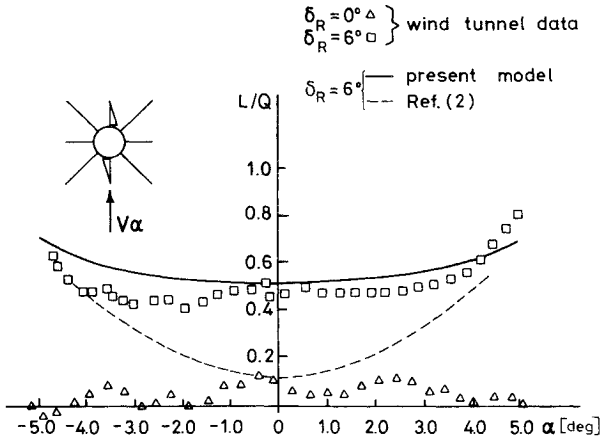

Fig. 10 Comparison of predicted rolling moment to experimental data for vertical canard deflection.

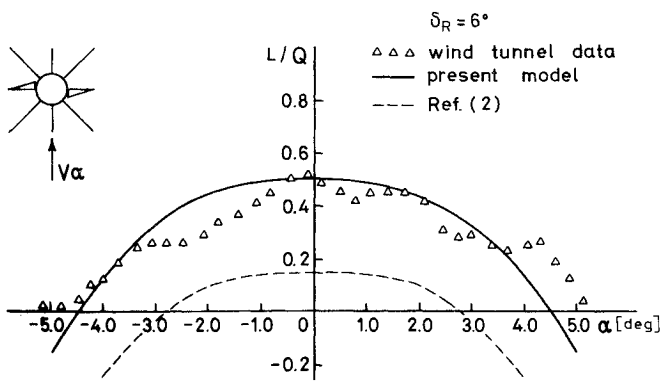

Fig. 11 Comparison of predicted rolling moment to experimental data for horizontal canard deflection.

Concluding Remarks

This paper presents an efficient computational method to predict the roll controllability of slender cruciform canard configurations. Comparison to experimental data has shown that the prediction is of good engineering accuracy. The satisfactory precision is due to two important improvements introduced into the mathematical model: 1) computing the trailing vortex trajectories under the influence of the tail surface; and 2) considering body interference on the rolling moment induced at the tail section.

The insight provided by the simple mathematical model and the nondimensional roll influence maps into the complex phenomenon of induced rolling moment makes this methodology very attractive for preliminary aerodynamic design of canard controlled configurations. The basic model also has an inherent capability, which has not yet been used, to predict induced lateral moments and forces due to canard deflection and angle of attack (or sideslip).

The simplifying assumptions and the experimental data used for comparison limit at the moment the domain of validity of the presented computation scheme to slender configurations and small angles of attack. The approach has, however, a definite potential for extension and further development. It can be used for higher angles of attack by adding appropriately computed body and leading-edge vortices. For configurations with no slender tail surfaces, computation of the roll influence function, performed by some more elaborate method, can be incorporated into the prediction procedure. Each type of extension requires, however, validation by comparison to experimental data.

Appendix: The Potential Induced by a Pair of Conjugate Vortices on a Circle

A vortex of strength Γ, placed at a point Σ_v, induced at any other point Σ in the plane a complex potential:

$$W=i(\Gamma/2\pi)\ln(\Sigma-\Sigma_v) \tag{A1}$$

If there is a solid circle of radius R at the origin in the flowfield, an image of this vortex has to be placed at Σ_I inside the circle satisfying

$$\Sigma_I=R^2/\Sigma_v \tag{A2}$$

The strength of the image vortex is $-\Gamma$.

The potential due to both vortices is

$$W=i(\Gamma/2\pi)\,[\ln(\Sigma-\Sigma_v)-\ln(\Sigma-\Sigma_I)] \tag{A3}$$

The potential induced on the circle of radius R (representing the contour of a cruciform tail-body combination) can be computed by substituting the values of Σ_v, Σ_I, and Σ:

$$\sigma_v=\Sigma_v/R=q_v\exp[i\phi_v]$$

$$\sigma_I=\Sigma_I/R=(1/q_v)\exp[i\phi_v]$$

$$\sigma=\Sigma/R=\exp[i\phi] \tag{A4}$$

into the equation of the potential (A3). Then

$$W=i(\Gamma/2\pi)\{\ln[R\exp(i\phi)-Rq_v\exp(i\phi_v)]$$

$$-\ln[R\exp(i\phi)-(R/q_v)\exp(i\phi_v)]\} \tag{A5}$$

Using the identity

$$\exp(i\phi)=\cos\phi+i\sin\phi \tag{A6}$$

gives:

$$W=i(\Gamma/2\pi)\{\ell n[(\cos\phi-q_v\cos\phi_v)+i(\sin\phi-q_v\sin\phi_v)] - \ell n[(\cos\phi-(1/q_v)\cos\phi_v)+i(\sin\phi-(1/q_v)\sin\phi_v)]\} \quad (A7)$$

A second identity

$$\Sigma=\eta+i\zeta=\sqrt{\eta^2+\zeta^2}\exp[i\tan^{-1}(\zeta/\eta)] \quad (A8)$$

yields

$$W=i\frac{\Gamma}{2\pi}\left(\ell n\left\{[(\cos\phi-q_v\cos\phi_v)^2+(\sin\phi-q_v\sin\phi_v)^2]^{1/2}\right\}\cdot\exp\left[i\tan^{-1}\left(\frac{\sin\phi-q_v\sin\phi_v}{\cos\phi-q_v\cos\phi_v}\right)\right] - \ell n\left\{\left[\left(\cos\phi-\frac{1}{q_v}\cos\phi_v\right)^2+\left(\sin\phi-\frac{1}{q_v}\sin\phi_v\right)^2\right]^{1/2}\right\}\cdot\exp\left[i\tan^{-1}\left(\frac{\sin\phi-(1/q_v)\sin\phi_v}{\cos\phi-(1/q_v)\cos\phi_v}\right)\right]\right) \quad (A9)$$

The complex potential is defined as

$$W\triangleq\Phi+i\psi \quad (A10)$$

where Φ is the potential and ψ is the stream function. Therefore, the potential Φ is given by

$$\Phi=\mathrm{Re}(W)=-\frac{\Gamma}{2\pi}\left[\tan^{-1}\frac{\sin\phi-q_v\sin\phi_v}{\cos\phi-q_v\cos\phi_v} - \tan^{-1}\frac{\sin\phi-(1/q_v)\sin\phi_v}{\cos\phi-(1/q_v)\cos\phi_v}\right] \quad (A11)$$

yielding after some trigonometrical manipulation,

$$\Phi=-\frac{\Gamma}{2\pi}\tan^{-1}\left\{\frac{[q_v-(1/q_v)]\sin(\phi-\phi_v)}{2-[q_v+(1/q_v)]\cos(\phi-\phi_v)}\right\} \quad (A12)$$

The normalized potential function

$$\Phi'=\frac{\Phi}{\Gamma/2\pi} \quad (A13)$$

is obtained finally as

$$\Phi'=-\tan^{-1}\left\{\frac{[q_v-(1/q_v)]\sin(\phi-\phi_v)}{2-[q_v+(1/q_v)]\cos(\phi-\phi_v)}\right\} \quad (A14)$$

References

[1] Shinar, J., "Roll Control Feasibility of a Slender Cruciform Configuration of Canard Surfaces at Mach Number 2.25," *Proceedings of the 16th Israel Annual Conference on Aviation and Astronautics; Israel Journal of Technology*, Vol. 12, 1974, pp. 31-39.

[2] Spreiter, J.R. and Sacks, A.H., "The Rolling up of the Trailing Vortex Sheet and Its Effect on Downwash behind Wings," *Journal of the Aeronautical Sciences*, Vol. 18, 1951, pp. 21-32.

[3] Edwards, S. and Hikido, K., "A Method for Estimating the Rolling Moment Caused by Wing-Trail Interference for Missiles at Supersonic Speeds," NACA RM A53H18, 1953.

[4] Gur, I., Shinar, J., and Rom, J., "A Method for the Evaluation of Induced Rolling Moments and Side Forces in Slender Cruciform Canard Configurations at Small Angles of Attack," *Proceedings of the 18th Israel Annual Conference on Aviation and Astronautics; Israel Journal of Technology*, Vol. 14, 1976, pp. 74-85.

[5] Spreiter, J.R. and Sacks, A.H., "A Theoretical Study of the Aerodynamics of Slender Cruciform Wing Arrangements and Their Wakes," NACA TN 3528, 1956.

[6] Sacks, A.H., "Aerodynamic Interference of Slender Wing-Trail Combinations," NACA TN 3725, 1957.

[7] Alskine, A.Y., "Determination of Vortex Paths by Series Expansion Technique with Application to Cruciform Wings," NACA TR 1311, 1957.

[8] Nielsen, J.N., *Missile Aerodynamics*, McGraw-Hill, New York, 1960.

[9] Udelson, D.G., "Vortex Induced Rolling Moments on Finned Missiles at High Angle of Attack," AFCRL-68-0569, 1968.

[10] Mendenhall, M.R. and Nielsen, J.N., "Effect of Symmetrical Vortex Shedding on the Longitudinal Aerodynamic Characteristics of Wing-Body-Tail Combinations," NASA CR-2473, 1975.

[11] Adams, G.T. and Dugan, D.W., "Theoretical Damping in Roll and Rolling Moment Due to Differential Wing Incidence for Slender Cruciform Wings and Wing-Body Combinations," NACA TR 1088, 1952.